



## Research paper

## Distributed fault-tolerant for leader-following multi-unmanned aerial vehicle systems with faulty sensors based on belief rule base

Ruohan Yang <sup>a,\*</sup>, Xiao Gong <sup>a</sup>, Zhichao Feng <sup>b</sup>, Yahui Hao <sup>c</sup><sup>a</sup> Northwestern Polytechnical University, Xi'an, 710072, PR China<sup>b</sup> Rocket Force University of Engineering, Xi'an, 710025, PR China<sup>c</sup> City University of Hong Kong, 999077, Hong Kong Special Administrative Region of China

## ARTICLE INFO

## Keywords:

Belief rule base  
 Multi-unmanned aerial vehicle systems  
 Sensor failure  
 Fault-tolerant control

## ABSTRACT

Effective fault-tolerant control (FTC) for leader-following Multi-Unmanned Aerial Vehicle (Multi-UAV) systems is crucial but challenging, especially when dealing with sensor faults in a distributed manner, including complex scenarios like overlapping failures leading to joint unobservability across multiple UAVs. This paper proposes a novel distributed FTC framework leveraging Belief Rule Base (BRB) combined with communication fusion (BRB-CF) to address these challenges. The framework integrates two key modules operating on each UAV: a decentralized BRB-based fault diagnosis (FD) module to accurately identify faulty sensor locations using local data, and a distributed reconstruction module utilizing BRB-CF. For non-overlapping faults, a communication-based fusion function compensates failures using neighbor data. Crucially, for overlapping faults where fusion is insufficient, a dedicated BRB-CF model reconstructs sensor outputs by integrating historical data with fused neighbor information. Simulation results demonstrate the proposed framework's effectiveness, enabling the multi-UAV system to maintain formation and performance stability under both non-overlapping and overlapping sensor fault conditions, thereby enhancing system robustness and resilience.

## 1. Introduction

Unmanned aerial vehicles (UAVs), commonly known as drones, have garnered significant attention in both civilian and military applications over recent decades. Their ability to perform a wide range of tasks, such as regional search and detection, cooperative transportation, and battlefield surveillance, has made them indispensable in various fields (AlMahamid and Grolinger, 2022). Unlike single UAVs, multi-UAV systems offer enhanced capabilities, including broader coverage, higher flexibility, and improved robustness. Furthermore, employing heterogeneous multi-UAV systems, where individual UAVs possess different dynamic characteristics, sensor payloads, or operational capabilities like endurance and speed, offers significant practical advantages. Such heterogeneity allows for optimized task allocation, where specific UAVs are assigned roles best suited to their design, leading to increased mission efficiency and cost-effectiveness (Wang et al., 2018). For example, a team might consist of UAVs specialized for high-resolution sensing alongside others optimized for communication relay or long endurance surveillance to monitor the target area efficiently (Queraltà et al., 2020). These advantages are especially crucial in large-scale operations, where the coordination of multiple UAVs is essential to

achieve efficiency and effectiveness. Large-scale deployment scenarios, such as post-disaster rescue missions and military reconnaissance, benefit greatly from the scalability and redundancy provided by multi-UAV systems (Baldini et al., 2023; Xu et al., 2023; Sun et al., 2025). For example, a team might consist of UAVs specialized for high-resolution sensing alongside others optimized for communication relay or long endurance surveillance to monitor the target area efficiently (Zhang et al., 2024a; Du et al., 2024; Wang et al., 2023).

However, the deployment of UAVs in dynamic and uncertain environments poses significant challenges, particularly in terms of system reliability and fault tolerance. The complex nature of UAV swarms, where each UAV's action can directly influence others, makes it crucial to ensure that the overall system remains robust, even in the event of component failures, such as sensor, actuator, or communication link faults (Guo and Ahn, 2020; Gong et al., 2022; Rotondo et al., 2023). Consequently, the development of FTC strategies that can accommodate such faults and maintain system performance is critical for the successful deployment of multi-UAV systems in real-world applications.

Traditional FTC techniques can be broadly classified into passive and active approaches. Passive FTC methods are designed to tolerate

\* Corresponding author.

E-mail addresses: [ruohanyang@nwpu.edu.cn](mailto:ruohanyang@nwpu.edu.cn) (R. Yang), [gongxiao@mail.nwpu.edu.cn](mailto:gongxiao@mail.nwpu.edu.cn) (X. Gong), [19BD04078@stu.hit.edu.cn](mailto:19BD04078@stu.hit.edu.cn) (Z. Feng), [yahuihao2-c@my.cityu.edu.hk](mailto:yahuihao2-c@my.cityu.edu.hk) (Y. Hao).

faults without modifying the controller. This approach is often developed from the observer-based perspective to passively isolate faults from the controller (Li et al., 2023; Yang et al., 2023b,a; Zou et al., 2020; Ahmadi et al., 2023). Observer-based passive fault-tolerant methods detect and isolate faults in multi-agent systems through residual evaluation and dynamic event-triggered control, ensuring robust consensus by limiting fault propagation without active intervention (Yang et al., 2023b,a). Active FTC methods involve real-time fault diagnosis and reconfiguration of the control system to compensate for faults (Zou et al., 2020; Ahmadi et al., 2023; Ma et al., 2023; Yang et al., 2024; Wang et al., 2022b; Shao and Ye, 2020; Zheng et al., 2021). Traditional control theories such as sliding mode control and adaptive control are widely used to achieve fault tolerance. Among these, adaptive control is particularly effective in managing uncertainties in system dynamics and external disturbances. For example, adaptive FTC strategies have been applied to systems with actuator faults, enabling dynamic adjustment of control parameters to maintain performance (Shao and Ye, 2020). Similarly, sliding mode control is employed in situations with abrupt system changes, such as loss of actuator effectiveness or sensor malfunctions. This method provides robustness by switching control actions to compensate for faults, ensuring system operation remains within safe limits (Zheng et al., 2021). However, traditional control theories primarily depend on precise dynamics, which often fail to work directly in practice due to the dynamics being unknown.

BRB systems have emerged as a tool for handling uncertainty and incomplete information in fault diagnosis and fault-tolerant control (Yang et al., 2006). Unlike traditional model-based approaches, BRB systems can manage complex, non-linear relationships between system variables, making them particularly suitable for applications where precise mathematical models are difficult to develop, or where expert knowledge significantly contributes to system operation (Feng et al., 2018). BRB integrates expert knowledge with observational data, offering a semi-quantitative approach that is both interpretable and flexible. In recent years, BRB systems have demonstrated superior performance in fault diagnosis, marine diesel engines, and system reliability assessment across various domains, including wireless sensor networks, industrial equipment (Feng et al., 2023a, 2020; Zhang et al., 2024d; Xu et al., 2017; Zhang et al., 2024c). A recent advancement in the BRB domain is its application in FTC for concurrent failures. Previously, BRB models were limited to single-event failures, but recent developments have facilitated frameworks capable of diagnosing simultaneous failures using an enhanced discernment frame. For example, the BRB-CE (Concurrent Events) model has been developed to address simultaneous sensor failures in wireless sensor networks, leveraging both expert knowledge and sensor data to diagnose faults and reconstruct outputs from failed sensors (Chang et al., 2020). Moreover, for multi-agent systems (MAS), a BRB model is also proposed as a decentralized fault diagnosis model for MAS using only relative neighbor information under external disturbances (Feng et al., 2023b).

In response to the aforementioned analysis, there are only a few works focused on the BRB-based distributed fault diagnosis and fault tolerance for multi-UAV systems. Moreover, the existing BRB-based FTC method (Chang et al., 2020) for the single system with single fault cannot be directly extended to the multi-UAV systems since the BRB-based FTC strategy equipped on each UAV cannot obtain the global information necessary for a cooperative fault-tolerant result. Therefore, this paper investigates BRB for multi-UAV systems subject to sensor faults by using signals transmitted from neighboring UAVs.

This paper makes several key contributions to the field of fault-tolerant control for multi-UAV systems, which are shown as follows.

- First, a distributed FTC framework based on BRB-CF is proposed, uniquely designed to operate with reduced model dependency by diagnosing faults and reconstructing necessary signals rather than estimating true values from faulty data, suitable for heterogeneous multi-UAV systems.

**Table 1**  
Description of mathematical notations.

Symbols	Description
$\mathbb{R}$	Real number system
$\mathbb{R}^n$	$n$ -dimensional Euclidean space
$\mathbb{R}^{m \times n}$	Set of $m \times n$ -dimensional real matrices
$\mathcal{G}$	Strongly connected graph
$\mathcal{A}$	Adjacency matrix
$L$	Laplacian matrix
$\in$	Element of, belongs to
$\ \cdot\ $	Norm of a vector or matrix
$\Sigma$	Summation
$\min$	Minimum

- Second, a novel BRB-CF-based reconstruction model is introduced, incorporating communication fusion and historical data intelligently based on fault type and joint observability conditions, enabling cooperative fault tolerance.
- Finally, the framework's applicability to non-linear multi-UAV systems, where the advantages of reduced model dependency are most pronounced, is demonstrated, offering a practical solution for real-world scenarios.

The paper is organized as follows: Section 2 presents preliminary knowledge of MAS systems and formulates the problem of sensor faults in leader-following multi-UAV systems. Section 3 details the construction of the proposed FTC framework. Section 4 includes a case study to demonstrate the method's performance. Finally, conclusions are drawn in Section 5.

## 2. Preliminary and problem formulation

### 2.1. Preliminary

Consider a directed strongly connected graph denoted by  $\mathcal{G} = \{\mathcal{V}, \mathcal{E}, \mathcal{A}\}$ , where  $\mathcal{V} = \{v_1, \dots, v_N\}$  represents a collection of  $N$  nodes corresponding to multiple UAVs. The set  $\mathcal{E} = \{\dots, (v_i, v_j), \dots\}$  consists of directed links, indicating the adjacency of two UAVs. The adjacency matrix,  $\mathcal{A} = [a_{ij}]$ , contains positive elements  $a_{ij}$  if there is information flow from UAV  $i$  to UAV  $j$ ; otherwise,  $a_{ij}$  is zero. The degree matrix, defined as  $\mathcal{D} = \text{diag}\{d_i\} \in \mathbb{R}^{N \times N}$ , has diagonal elements  $d_i$  that represent the sum of  $a_{ij}$  over  $j$  belonging to the set  $N_i$  of adjacent nodes to UAV  $i$ . This set is expressed as  $N_i = \{j \in \mathcal{V} : (i, j) \in \mathcal{E}\}$ . The graph Laplacian, denoted by  $L$ , is given by  $L = \mathcal{D} - \mathcal{A}$ . This matrix  $L$  characterizes the directed graph and satisfies the property  $L\mathbf{1}_N = \mathbf{0}$ , where  $\mathbf{1}_N$  is an  $N$ -dimensional column vector with all entries equal to one (see Table 1).

**Remark 1.** In this paper, the communication graph  $\mathcal{G}$  among the UAVs is assumed to be a directed strongly connected graph. This assumption ensures that information can propagate throughout the network, which is essential for the distributed estimation and fault compensation mechanisms employed in the proposed FTC framework. The weights  $a_{ij} > 0$  if there is a communication link from UAV  $i$  to UAV  $j$ ; otherwise,  $a_{ij} = 0$ . Similar assumptions on graph connectivity and communication link weights can be found in the works on distributed control for multi-agent systems (Yang and Dong, 2024; Han et al., 2018).

### 2.2. Problem formulation

Consider a group of heterogeneous UAVs with a leader and  $N$  followers. The dynamics of each UAV can be described by the following general form:

$$\begin{aligned} \dot{x}_i(t) &= f_i(x_i(t), u_i(t)), \\ y_i(t) &= \phi_i(x_i(t)), \end{aligned} \quad (1)$$

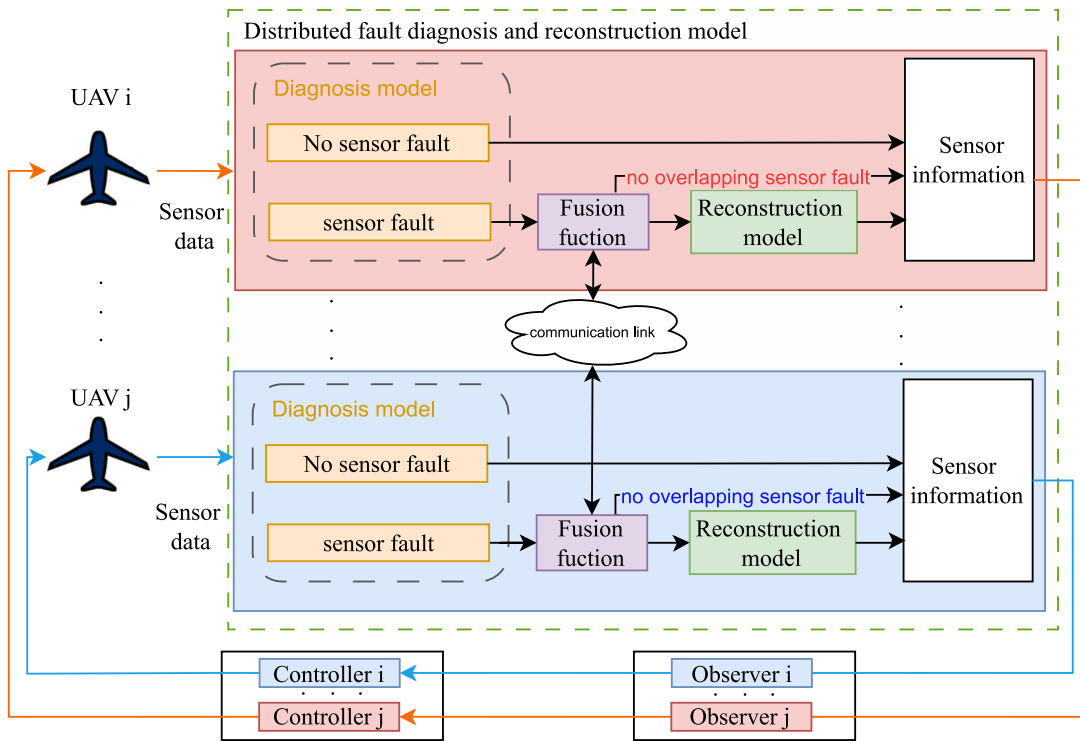


Fig. 1. Distributed fault-tolerant control framework.

where  $x_i(t) \in \mathbb{R}^{n_x}$  denotes the state of UAV  $i$ , and  $y_i(t) \in \mathbb{R}^{n_y}$  represents the output of UAV  $i$ . The term  $u_i(t)$  denotes the control input of UAV  $i$ . The functions  $f_i(\cdot)$  and  $\phi_i(\cdot)$  are nonlinear functions characteristic of the UAV, where  $i = 0, 1, \dots, N$ .

In this context, it is assumed that all follower UAVs are equipped with sensors to observe the output of the leader UAV. This setup results in a substantial replication of sensors observing the leader's output across the follower UAVs. For example, for each dimension of the leader UAV's output, there is a corresponding sensor on each follower UAV. Consequently, for all  $N$  follower UAVs, each dimension of the leader UAV's output is observed by  $N$  sensors distributed across all the followers.

Based on the foundational knowledge, we introduce the definition of sensor faults. When some sensors on UAV  $i$  fail, the observation data from the leader UAV to follower UAV  $i$  can be expressed as:

$$\hat{y}_i(t) = M_i(t)y_0(t), \quad (2)$$

where  $\hat{y}_i(t)$  represents the partial output observed by the  $i$ th follower UAV.  $M_i(t) = \text{diag}(m_1(t), \dots, m_{n_y}(t))$  is the time-varying faulty output matrix, with  $0 \leq m_p(t) \leq 1$  for  $p = 1, \dots, n_y$ . Furthermore,  $F_i = M_i F$  denotes the faulty sensor matrix.

**Remark 2.** The multiplicative fault model (2), using an unknown and time-varying matrix  $M_i$ , is commonly adopted in Rotondo et al. (2023) and Yadegar and Meskin (2021). In this work, it primarily represents loss of effectiveness sensor faults, such as gain degradation, reflecting realistic dynamics. The objective of the proposed FTC framework is to detect and compensate for the effects of this unknown loss of effectiveness characterized by  $M_i$ .

**Remark 3.** Significant advancements address challenging faults using model-based techniques, exemplified by recent works from Han et al. (2023a,b) tackling finite-time estimation and FTC for switched fuzzy systems with large, fast, or unbounded faults via sophisticated observer designs reliant on precise system models. Our distributed BRB-CF framework offers a contrasting philosophy, alleviating strong

model dependency by integrating qualitative expert knowledge and quantitative operational data (Yang et al., 2006; Feng et al., 2018). This is advantageous for complex non-linear multi-UAV systems where accurate modeling is difficult. While these model-based approaches excel at handling specific dynamics like unboundedness (Han et al., 2023a,b), our current work focuses on multiplicative loss-of-effectiveness sensor faults. Extending our knowledge-data driven BRB framework to handle a broader range of fault types, such as bias, drift, unboundedness, and incorporate concepts like finite-time performance, potentially combining paradigm strengths, remains important future research.

To ensure that the followers can track the leader, provided that the leader's dynamics are observable, the controllers for the UAVs are designed as:

$$u_i(t) = k_i(x_i(t), \bar{y}_i(t)), \quad (3)$$

where  $k_i$  is the function that needs to be designed for formation performance.  $\bar{y}_i(t)$  is the reconstructed sensor data produced by the fault tolerant strategy to be designed.

**Assumption 1.** The dynamic model of each UAV is assumed to be controllable and observable.

**Definition 1 (Formation).** Consider a multi-UAV system (1) with a direct strongly connected communication graph  $G$ . Let  $h_i \in \mathbb{R}^{n_x}$  be the desired constant relative state vector for follower UAV  $i$  with respect to the leader, and let  $h = [h_1^T, h_2^T, \dots, h_N^T]^T$  be the concatenated vector representing the desired formation configuration. If there exists a controller  $u_i$  such that the following condition is satisfied:

$$\lim_{t \rightarrow \infty} \|x_i(t) + h_i - x_0(t)\| = 0, \quad i = 1, 2, \dots, N, \quad (4)$$

then the multi-UAV system is considered to achieve formation.

In practical applications, sensor failures can cause observation data of UAVs to collapse, resulting in significant deviations from the actual data of the leader UAV's state and disrupting formation control. While many existing fault-tolerant control methods address sensor faults,

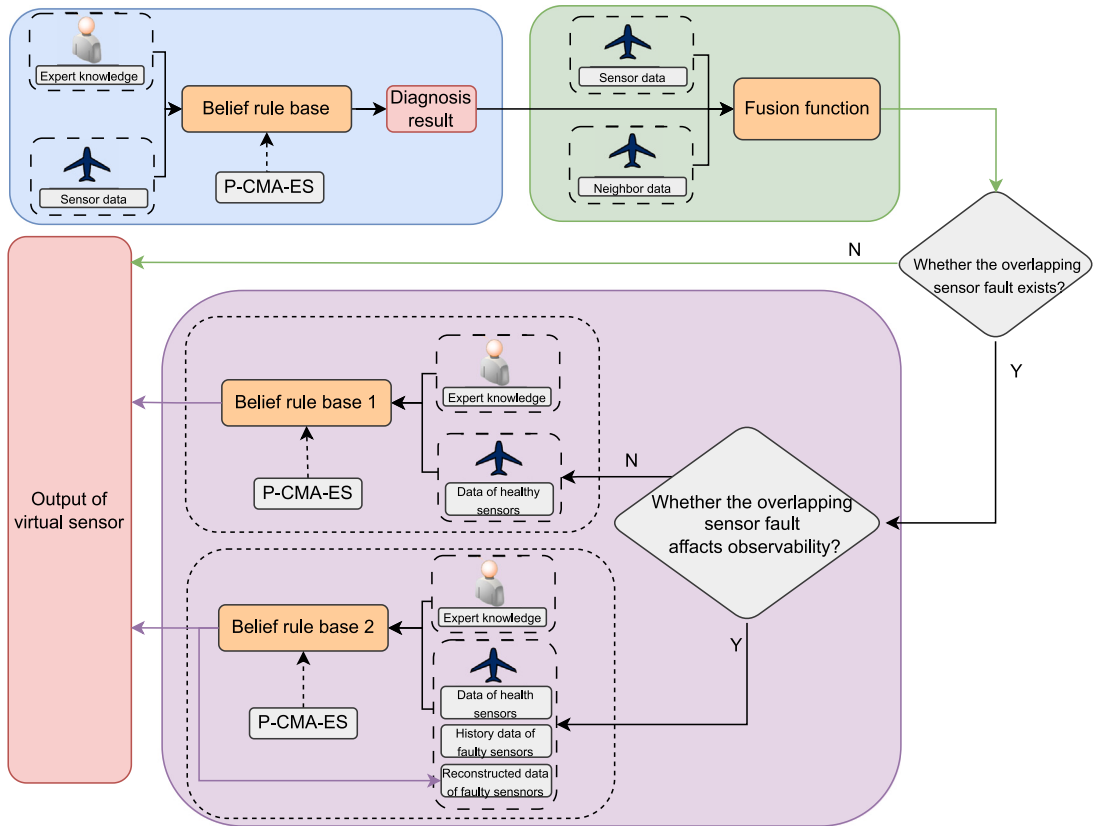


Fig. 2. Decentralized fault diagnosis and distributed reconstruction model.

often relying on reconstructing the leader's signal using observers (Yang and Dong, 2024; Han et al., 2018), these prevalent approaches face several limitations in the context of complex multi-UAV systems. Firstly, they frequently depend on strict observability conditions regarding the leader's state from individual follower measurements, an assumption only recently relaxed in specific contexts (Yang and Dong, 2024; Han et al., 2018). Secondly, their effectiveness heavily relies on the accuracy of the underlying system model used for observer design (Yang and Dong, 2024), yet obtaining precise dynamic models for sophisticated UAVs is often challenging. Finally, although Belief Rule Base (BRB) methods have shown promise for reconstruction (Feng et al., 2023b), existing applications are typically limited to single systems, neglecting the potential benefits and complexities of information fusion among multiple interacting UAVs.

To address these challenges and develop a more robust and practical distributed FTC framework, two interconnected subproblems need to be solved:

**Subproblem 1 (Decentralized Fault Diagnosis).** It is essential to incorporate a distributed and embedded fault diagnosis module within each UAV. This module facilitates the timely detection and identification of sensor failures, which is a prerequisite for activating appropriate fault-tolerant actions. However, developing such a diagnostic system faces practical difficulties, notably the inherent uncertainty often present in expert diagnostic knowledge and the common issue of imbalanced datasets, where data representing faulty conditions is much scarcer than data from normal operation.

**Subproblem 2 (Distributed Fault-Tolerant Signal Reconstruction).** Following a positive fault diagnosis, the core task of FTC is to provide the control system with a reliable substitute for the compromised sensor information. To relax observability requirements and enhance robustness, this should involve reconstructing the necessary sensor output signal by

intelligently utilizing information exchanged with neighboring UAVs. This reconstruction task is challenging because model-based methods suffer from the aforementioned model inaccuracies, while purely data-driven approaches struggle due to the lack of sufficient and diverse fault data needed to train reliable reconstruction models, especially given the data imbalance issue highlighted in Subproblem 1.

The unique combination of challenges, including uncertain expert knowledge, imbalanced data, and model uncertainty, strongly motivates the adoption of the Belief Rule Base (BRB) methodology for both diagnosis and reconstruction. As a knowledge-data hybrid approach (Yang et al., 2006; Feng et al., 2018), BRB is adept at integrating potentially uncertain expert rules with available, even limited or imbalanced, operational data. Therefore, to tackle the specific issues outlined in the subproblems above, this paper proposes the development of a decentralized BRB-based fault diagnosis model and a distributed fault reconstruction method based on BRB with Communication Fusion (BRB-CF). The detailed construction of these components is presented in Section 3.

### 3. Construction of distributed FTC framework

This section explores the construction of the distributed FTC framework, integrating the FD module and reconstruction model. Section 3.1 introduces the BRB-based FD model, which is designed to detect and diagnose sensor faults for each UAV. Section 3.2 outlines the development of a distributed BRB-based fault reconstruction model aimed at reconstructing faulty sensors by using different BRB models aligned with the observability of the remaining healthy sensors. Finally, Section 3.3 presents the optimization model for the comprehensive FTC framework, enhancing its efficiency.

The overall architecture of the proposed distributed FTC framework is depicted in Fig. 1. It highlights the key components within each UAV, including the local sensors, the decentralized BRB-based fault diagnosis

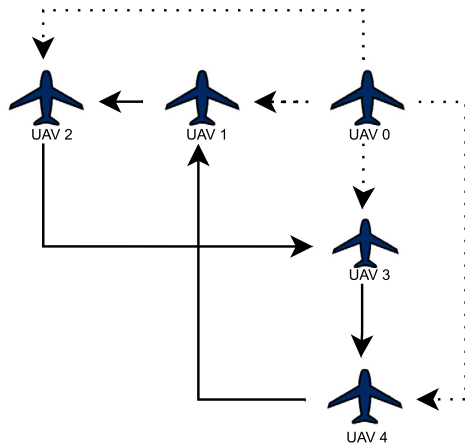


Fig. 3. The communication graph representing the interconnections among UAVs.

module, the communication interface for neighbor data exchange, the BRB-CF-based reconstruction module, and the UAV controller.

### 3.1. BRB-based decentralized fault diagnosis model

The BRB methodology, a knowledge-data hybrid driven method, provides a framework for modeling complex systems under uncertainty. It utilizes a set of belief rules that map antecedent inputs, such as sensor readings, to a belief distribution across consequent outputs, such as system states or fault diagnoses. Each rule captures expert knowledge or learned patterns. A key strength of BRB is its ability to effectively integrate these sources, functioning as a hybrid model driven by both qualitative expert insights and quantitative observational data, even when available data is limited. Then, the outputs of activated rules based on input evidence are aggregated by an evidential reasoning algorithm to produce a final assessment. This ability to explicitly represent and reason with uncertainty makes BRB particularly suitable for decentralized fault diagnosis tasks. In this section, we detail the construction of a distributed BRB-based FD model for each UAV.

To identify the operational status (healthy or faulty) of each individual sensor equipped on a UAV, a dedicated BRB-based FD model is constructed and executed locally on each UAV. Assuming UAV  $i$  has  $n_y$  sensors measuring the leader's output dimensions (or other relevant variables), its local FD model takes the readings from all its own sensors ( $\hat{y}_{i1}(t), \dots, \hat{y}_{in_y}(t)$ ) as input. The goal of this model is to output a diagnosis result indicating the status of each of these  $n_y$  sensors. Taking follower UAV  $i$  as an example, the basic structure of the  $k$ th belief rule within its local FD model is outlined as:

$$R_k(t) : \text{If } \hat{y}_{i1}(t) \text{ is } A_1^k \wedge \hat{y}_{i2}(t) \text{ is } A_2^k \wedge \dots \wedge \hat{y}_{in_y}(t) \text{ is } A_{n_y}^k,$$

then  $F(t)$  is  $\{\Theta_1, \beta_{1,k}, \dots, \Theta_Q, \beta_{Q,k}\}$

with rule weight  $\lambda_k$ , attribute weight  $\delta_{i1}, \dots, \delta_{in_y}$ .

where  $\hat{y}_{is}(t)$  for  $s = 1, \dots, n_y$  represents the observational data from all sensors associated with follower UAV  $i$ , and  $n_y$  denotes the total number of sensors on UAV  $i$ . The reference value of  $\hat{y}_{is}(t)$  in  $R_k(t)$  is indicated by  $A_s^k$  for each  $s = 1, \dots, n_y$ . Diagnosis events are denoted as  $\{\Theta_1, \Theta_2, \dots, \Theta_Q\}$ . The belief degree corresponding to each element in the BRB output is represented by  $\beta_{q,k}$  for  $q = 1, \dots, Q$ . The significance of the  $k$ th belief rule  $R_k(t)$  is denoted by its weight  $\lambda_k$ , while the attribute weight  $\delta_{is}$  for  $s = 1, \dots, n_y$  represents the importance of  $\hat{y}_{is}(t)$  under rule  $R_k(t)$ . Initially, both  $\lambda_k$  and  $\delta_{is}$  are determined based on empirical expertise.

With the foundational model established, the inference process of the BRB-based FD model involves the following steps:

Step 1: Calculate the matching degree of the attributes.

For scenarios where all sensor data inputs are available, the matching degree for the  $s$ th sensor data in the  $m$ th rule  $\alpha_s^m$  is calculated as follows:

$$\alpha_s^m = \begin{cases} \frac{\hat{y}_{is(k+1)} - \hat{y}_{is}(t)}{\hat{y}_{is(k+1)} - \hat{y}_{is}(t)} & m = k \text{ if } \hat{y}_{is(k)} \leq \hat{y}_{is}(t) \leq \hat{y}_{is(k+1)} \\ \frac{\hat{y}_{is}(t) - \hat{y}_{is(k)}}{\hat{y}_{is(k+1)} - \hat{y}_{is}(t)} & m = k + 1 \\ 0 & m = 1, 2, \dots, L, m \neq k, k + 1 \end{cases} \quad (5)$$

where  $\hat{y}_{is(k+1)}$  and  $\hat{y}_{is(k)}$  are the reference points for the sensor  $s$ 's output of UAV  $i$  for the  $k$ th and  $(k+1)$ th rules, predetermined by experts. The current sensor data input for UAV  $i$  is represented by  $\hat{y}_{is}(t)$ . The rule is activated when the matching degree for sensor  $s$  on UAV  $i$  is non-zero. Here,  $L$  symbolizes the total number of rules within the BRB model.

Moreover, the input matching degree for the  $k$ th rule is computed as follows:

$$\alpha_k = \prod_{s=1}^{n_y} (\alpha_s^k)^{\delta_s} \quad (6)$$

where  $n_y$  represents the number of sensors on the UAV in the  $k$ th rule.  $\delta_s$  denotes the relative weight of the  $s$ th sensor of UAV  $i$  and is calculated by:

$$\bar{\delta}_s = \frac{\delta_s}{\max_{s'=1, \dots, n_y} \{\delta_{s'}\}}, \quad 0 \leq \bar{\delta}_s \leq 1 \quad (7)$$

Step 2: Calculate the activation weight of the belief rule.

The activation weight of the  $k$ th rule is determined by:

$$w_k = \frac{\theta_k \alpha_k}{\sum_{l=1}^L \theta_l \alpha_l}, \quad k = 1, \dots, L \quad (8)$$

where  $w_k$  is the activation weight of the  $k$ th rule. The weight  $\theta_k$  of the  $k$ th rule is initially set by experts and can be modified through an optimization model.

Step 3: Fuse the activated rules and calculate the belief degree using ER algorithm. Assuming  $L$  rules are potentially activated with activation weights  $w_k$ , the ER algorithm is used to fuse the belief distributions from these rules. The normalization factor  $\mu$  is calculated first:

$$\mu = \left[ \sum_{q=1}^Q \prod_{k=1}^L (w_k \beta_{q,k} + 1 - w_k \sum_{q=1}^Q \beta_{q,k}) - (Q-1) \prod_{k=1}^L (1 - w_k \sum_{q=1}^Q \beta_{q,k}) \right]^{-1} \quad (9)$$

Using this normalization factor, the fused belief degree  $\beta_q$  for the  $q$ th diagnosis event  $\Theta_q$  is given by:

$$\beta_q = \frac{\mu [\prod_{k=1}^L (w_k \beta_{q,k} + 1 - w_k \sum_{q=1}^Q \beta_{q,k}) - \prod_{k=1}^L (1 - w_k \sum_{q=1}^Q \beta_{q,k})]}{1 - \mu [\prod_{k=1}^L (1 - w_k)]} \quad (10)$$

where  $\beta_q$  represents the belief degree of the  $q$ th diagnosis event.

Step 4: Calculate the diagnosis output of the FD model.

The final step involves translating the aggregated belief degree vector  $B(t) = [\beta_1, \beta_2, \dots, \beta_Q]$  obtained from Step 3 into a definitive diagnosis result for UAV  $i$ . This is achieved using proximity classification against predefined failure threshold vectors.

It should be noted that each UAV is equipped with a dedicated BRB based fault diagnosis module. Within this module, a set of failure threshold vectors  $J_n$  ( $1 \leq n \leq Q$ ) is defined. Each vector  $J_n$  represents the ideal belief distribution corresponding to a specific diagnosis event  $\Theta_n$  (e.g., a particular sensor or combination of sensors being faulty or healthy). For instance, if  $\Theta_n$  represents only sensor 1 failing,  $J_n$  might be  $[1, 0, \dots, 0]$ , assuming  $\beta_1$  corresponds to the belief in  $\Theta_1$ .

To identify the most likely diagnosis event based on the calculated belief vector  $B(t)$ , we find the threshold vector  $J_r$  that is closest to  $B(t)$  in terms of Euclidean distance, formulated as:

$$\|B(t) - J_r\| = \min_{1 \leq r \leq Q} \|B(t) - J_r\| \quad (11)$$

The index  $r$  identifies the closest threshold vector  $J_r$ , indicating that the diagnosis event  $\Theta_r$  is considered the most plausible outcome.

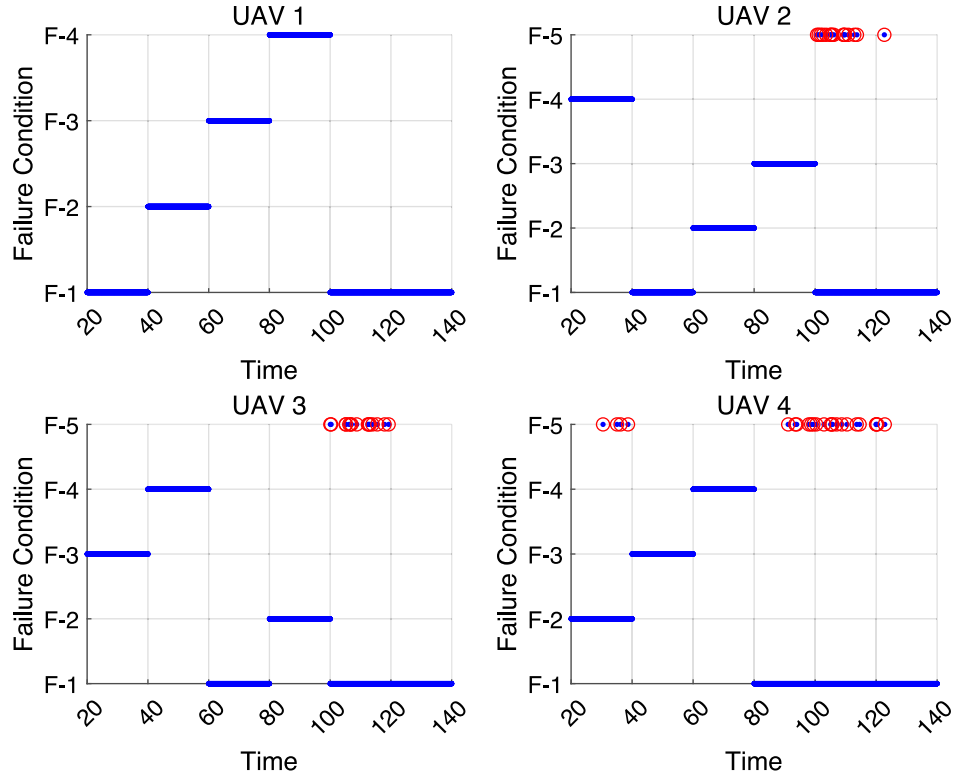


Fig. 4. Diagnosis result of all UAVs using FD module.

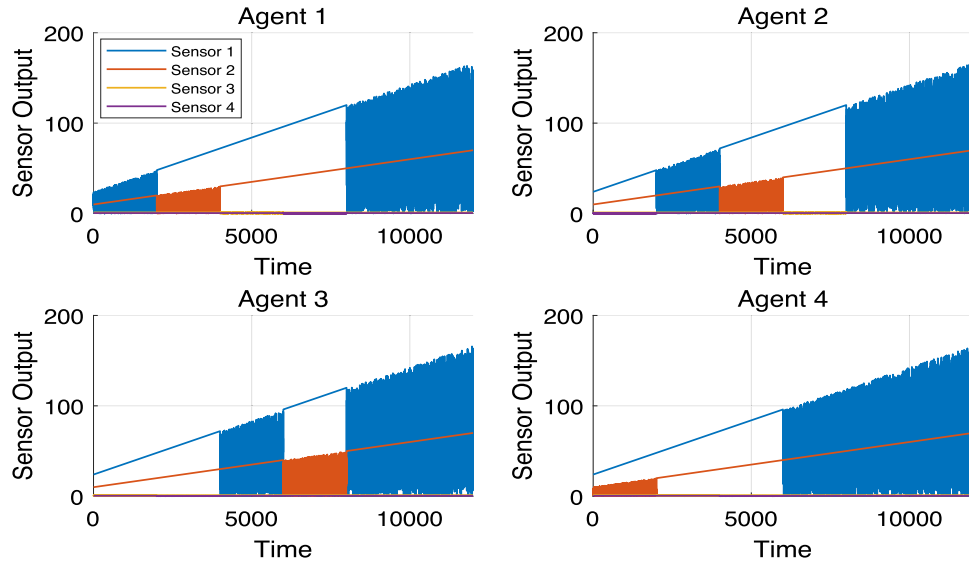


Fig. 5. Fault injection for 4 follower UAVs.

Finally, this identified diagnosis event  $\Theta_r$  is mapped to the binary diagnosis vector  $b_i = [b_{i1}, \dots, b_{is}, \dots, b_{in_y}]$  for UAV  $i$ . The mapping rule is as follows: if the event  $\Theta_r$  indicates that the  $s$ th sensor is healthy, then the corresponding element  $b_{is}$  is set to 1. Conversely, if  $\Theta_r$  indicates that the  $s$ th sensor is faulty, then  $b_{is}$  is set to 0. This vector  $b_i$  explicitly identifies the diagnosed status (healthy or faulty) and thus the location of any faulty sensors on UAV  $i$ .

For example, if there are two sensors equipped on a UAV, the diagnosis events can be written as  $\{\Theta_1, \Theta_2, \Theta_3, \Theta_4\} = \{I, II, \{I \wedge II\}, N_{12}\}$ , where  $I$  means sensor 1 is failure, i.e.,  $b_{i1} = 0$ ,  $II$  means sensor 2 is failure,  $\{I \wedge II\}$  means both of sensors 1 and 2 are failure, and  $N_{12}$

means both of sensors 1 and 2 are healthy. According to the diagnosis events, the failure threshold vectors of sensor faults can be written as  $J_1 = \{1, 0, 0, 0\}$ ,  $J_2 = \{0, 1, 0, 0\}$ ,  $J_3 = \{0, 0, 1, 0\}$ ,  $J_4 = \{0, 0, 0, 1\}$ . If the output vector  $B(t)$  of FD module is closest to  $J_1$ , then the actual failure vector is  $J_r = J_1$ , and the belief degree of diagnosis event  $\Theta_1$  is 1. Then, it can be observed that sensor 1 is failure, and sensor 2 is healthy, i.e.,  $b_{i1} = 0$  and  $b_{i2} = 1$ .

**Remark 4.** In order to achieve accurate fault diagnosis, it is necessary to construct the model of fault exactly. There are two main methods to construct the fault model, the one is utilizing expert knowledge, and

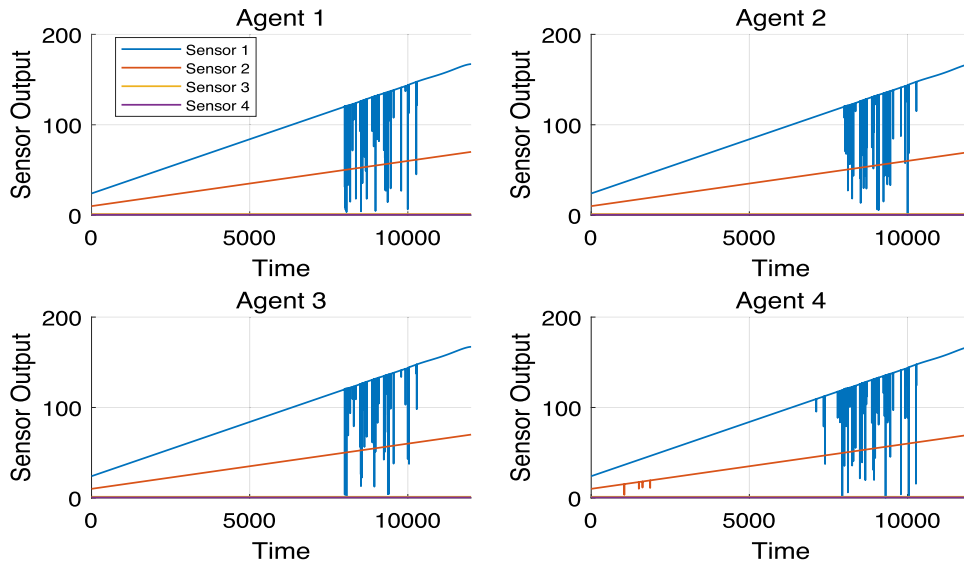


Fig. 6. Reconstructed sensor using proposed FTC.

the other is analyzing the relationship between fault and the indicators by using sufficient high-quality labeled data. However, in practical applications, uncertain expert knowledge for multi-UAVs and the unbalanced data between healthy and faulty status of UAVs will affect the accuracy of fault diagnosis. It should be noted that the proposed BRB-based fault diagnosis module, as a knowledge-data hybrid driven method, could make full use of the expert knowledge and unbalanced data, and ensure the diagnostic accuracy of sensor faults.

### 3.2. BRB-based distributed faulty sensor reconstruction model

Once the local fault diagnosis module, detailed in Section 3.1, identifies potential sensor faults through the indicator  $b_i$ , the next stage involves reconstructing reliable sensor data  $\bar{y}_i(t)$  for the control system. This reconstruction process leverages both local information and data exchanged with neighboring UAVs. Fig. 2 illustrates the workflow within a single UAV for this reconstruction phase. The following subsections detail the construction of the BRB-CF model and the specific input fusion strategy employed.

#### 3.2.1. Construction of BRB-CF

In this subsection, a distributed reconstruction model based on the BRB-CF is designed specifically for reconstructing the states of faulty sensors. Traditional BRB models lack the capability to interact with other BRBs to produce cooperative outputs, rendering them unsuitable as replacements for traditional distributed observers based on graph topology (Yang and Dong, 2024; Han et al., 2018). Therefore, a fusion function is crucial to assimilate local information, which includes local sensor data and local fault diagnosis outputs, and neighbor information, encompassing neighbor sensor data and neighbor fault diagnosis outputs. This fusion function is articulated as:

$$\tilde{y}_{ip}(t) = \mathcal{F} \{ b_{ip}(t), \hat{y}_{ip}(t), b_{jp}(t), \hat{y}_{jp}(t), \dots \} \\ (p = 1, \dots, n_y, j = 1, \dots, N_i)$$

where  $\tilde{y}_{ip}(t)$  signifies the fused sensor data incorporating healthy sensor data from all other UAVs accessible to UAV  $i$  through the graph topology.

The fused observation data and its corresponding diagnosis result are subsequently incorporated into our distributed faulty sensor reconstruction model based on BRB-CF.

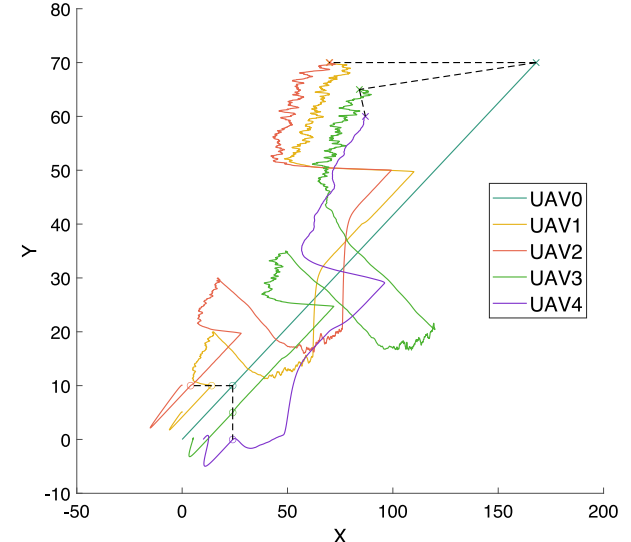


Fig. 7. Formation of 20–140 s under failure.

**Definition 2.** Let the fused observation provide healthy dimensions of fused observation data  $\bar{y} = [\bar{y}_1, \dots, \bar{y}_{p-1}, 0, \bar{y}_{p+1}, \dots, \bar{y}_{q-1}, 0, \dots, \bar{y}_{q+1}, \dots, \bar{y}_{n_y}]$ . It is deemed observable by follower UAV  $i$  from the leader UAV's output if:

$$\text{rank}(\mathcal{O}(x_0)) = \begin{pmatrix} \frac{\partial \bar{y}}{\partial x_0} \\ \frac{\partial (L_f \bar{y})}{\partial x_0} \\ \vdots \\ \frac{\partial (L_f^{n-1} \bar{y})}{\partial x_0} \end{pmatrix} = n$$

where  $n$  is the dimension of the state  $x_0$ .

**Case 1: Observability** is satisfied for the fused observation data.

In this scenario, if the fused observation data fulfills the condition of observability, then the fused observation from UAV  $i$  suffices for the BRB-based construction model. Assuming there are overlapping faulty sensors  $p, \dots, q$ , the output of the  $p$ th overlapping faulty sensor of UAV  $i$  at time  $t$  can be derived using the following BRB-CF based reconstruction model:

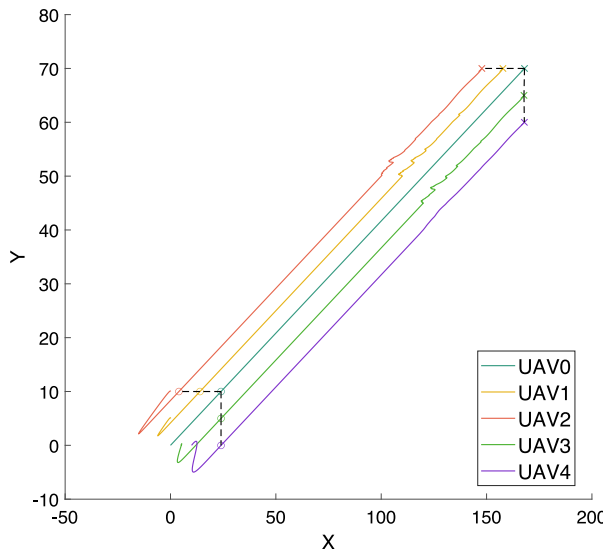


Fig. 8. Formation of 20–140 s using proposed FTC.

$R_1^{p,k}$  : If  $\tilde{y}_{i1}(t)$  is  $A_1^k \wedge \dots \wedge \tilde{y}_{i(p-1)}(t)$  is  $A_{p-1}^k \wedge \tilde{y}_{i(p+1)}(t)$  is  $A_p^k$   $\wedge \dots \wedge \tilde{y}_{in_y}(t)$  is  $A_{n_y}^k$   
is  $A_{p+1}^k \wedge \dots \wedge \tilde{y}_{i(q-1)}(t)$  is  $A_{q-1}^k \wedge \tilde{y}_{i(q+1)}(t)$  is  $A_q^k$   
then  $\tilde{y}_{ip}(t)$  is  $\{(D_1^p, \beta_{1,k}^p), \dots, (D_E^p, \beta_{E,k}^p)\}$ ,  
with rule weight  $\zeta_k^p$ , sensor weight  $\tau_{1,p}$ ,  
 $\dots, \tau_{p-1,p}, \tau_{p+1,p}, \dots, \tau_{q-1,p}, \tau_{q+1,p}, \dots, \tau_{n_y,p}$ .

where  $R_1^{p,k}$  denotes the  $k$ th belief rule of the reconstruction model for the  $p$ th sensor of follower UAV  $i$  in case 1. The terms  $D_1^p, \dots, D_E^p$  represent the reference points of  $p$ th sensor, and  $E$  denotes the number of reference points. The variables  $\tau_{1,p}, \dots, \tau_{p-1,p}, \tau_{p+1,p}, \dots, \tau_{q-1,p}, \tau_{q+1,p}, \dots, \tau_{n_y,p}$  are weights assigned to the health sensors' data among follower UAV  $i$ .

The inference process of the BRB-CF-based output reconstruction model for a single sensor failure is similar to the BRB-based FD model. The primary difference lies in the rule fusion mechanism. In the output reconstruction model for a single sensor failure, the activated rules are aggregated using the ER algorithm, which can be expressed as follows:

$$\beta_e^p = \frac{\mu'[\prod_{k=1}^L (w_k \beta_{e,k}^p + 1 - w_k \sum_{e=1}^E \beta_{e,k}^p) - \prod_{k=1}^L (1 - w_k \sum_{e=1}^E \beta_{e,k}^p)]}{1 - \mu'[\prod_{k=1}^L (1 - w_k)]} \quad (12)$$

$$\mu' = \left[ \sum_{e=1}^E \prod_{k=1}^L (w_k \beta_{e,k}^p + 1 - w_k \sum_{e=1}^E \beta_{e,k}^p) - (E-1) \prod_{k=1}^L (1 - w_k \sum_{e=1}^E \beta_{e,k}^p) \right]^{-1} \quad (13)$$

where  $L$  represents the number of rules in the output reconstruction model for the  $p$ th faulty sensor. The variable  $\beta_e^p$  refers to the output belief degree of the  $e$ th reference point  $D_e^p$ . The term  $w_k$  signifies the activation weight of the  $k$ th rule in the output reconstruction model.

The reconstructed output  $\tilde{y}_{ip}(t)$  is calculated as the expected value based on the combined belief degrees  $\beta_e^p$  and the corresponding numerical reference point values  $\mu_e^p$ , where  $D_e^p$  represents the linguistic term and  $\mu_e^p$  its quantitative value. This provides the final numerical estimate for the faulty sensor's reading at time  $t$ .

$$\tilde{y}_{ip}(t) = \sum_{e=1}^E \beta_e^p \mu_e^p \quad (14)$$

Case 2: Observability is not satisfied for the fused observation data

In scenarios where overlapping sensor faults are severe enough that the fused observation data  $\tilde{y}_i(t)$  does not satisfy the observability condition defined in [Definition 2](#), relying solely on this fused data is insufficient for accurate reconstruction. The fused data in this context contains only currently available healthy sensor information from neighbors. To address this, the BRB-CF reconstruction model for Case 2 incorporates historical information from the previously faulty sensors alongside the currently available fused healthy sensor data.

Specifically, to reconstruct the output  $\tilde{y}_{ip}(t)$  of the  $p$ th overlapping faulty sensor of UAV  $i$  at time  $t$ , the following BRB-CF based reconstruction model is used. Let  $P = \{p, \dots, q\}$  be the set of indices corresponding to the overlapping faulty sensors at time  $t$ , and let  $H = \{f, \dots, g\}$  be the set of indices for the currently healthy sensors, based on the fused diagnosis  $\tilde{b}_i(t)$ . The  $k$ th belief rule for reconstructing the  $p$ th sensor's output in this case, denoted  $R_2^{p,k}$ , takes the form:

$R_2^{p,k}$  : If  $\wedge_{s \in P} (\tilde{y}_{is}^r(t-1) \text{ is } A_s^k) \wedge_{h \in H} (\tilde{y}_{ih}(t) \text{ is } A_h^k)$   
then  $\tilde{y}_{ip}(t)$  is  $\{(D_1^p, \eta_{1,k}^p), \dots, (D_E^p, \eta_{E,k}^p)\}$ ,  
with rule weight  $\rho_k^p$ , and attribute weights  $\{\nu_{s,p}\}_{s \in P \cup H}$ .

where the antecedent combines conditions based on two distinct types of inputs. The first type is the historical input from previously faulty sensors, denoted as  $\tilde{y}_{is}^r(t-1)$  for each index  $s$  in the set  $P$ . The value  $\tilde{y}_{is}^r(t-1)$  is determined by the crucial feedback mechanism designed to mitigate error accumulation. The terms  $A_s^k$  and  $A_h^k$  are the reference values for the respective historical and current attributes in the  $k$ th rule. The consequent provides a belief distribution over possible output values  $\{D_1^p, \dots, D_E^p\}$  for the  $p$ th sensor, with belief degrees  $\eta_{e,k}^p$ . The parameters  $\rho_k^p$ , the rule weight, and  $\nu_{s,p}$ , the attribute weights for both historical and current inputs, govern the inference process for this Case 2 BRB model. The inference process of case 2 belief rule base is similar to case 1.

The feedback mechanism designed to mitigate error accumulation is defined as:

$$\tilde{y}_{is}^r(t-1) = \begin{cases} \tilde{y}_{is}(t-1), & \text{if sensor } s \text{ was diagnosed healthy at } t-1, \\ \bar{y}_{is}(t-1), & \text{if sensor } s \text{ was diagnosed faulty at } t-1. \end{cases} \quad (15)$$

where  $\tilde{y}_{is}(t-1)$  is the fused sensor data and  $\bar{y}_{is}(t-1)$  is the reconstructed output for sensor  $s$  at the previous instant  $t-1$ . This selection ensures the model uses the best available estimate from the past. The inference process of case 2 belief rule base is similar to case 1.

### 3.2.2. Input fusion

In this subsection, we introduce a straightforward fusion function to further investigate the BRB-CF based distributed faulty sensor reconstruction model.

Step 1: Each UAV independently produces a diagnosis result.

Each UAV is equipped with a BRB-based FD module for all sensors.

The diagnostic result for UAV  $i$  is denoted as  $b_i$ .

Step 2: Receive data from neighbor UAVs.

Assuming a communication framework is established based on the strongly connected graph of the multi-UAV system, UAV  $i$  is expected to receive two types of data: (1) the observation data from the neighboring UAVs  $j \in N_i$ , and (2) the diagnostic result from the BRB-based FD module hosted by the input neighbors  $j \in N_i$ .

The fusion function output for UAV  $i$  is formulated as follows:

$$\tilde{y}_{ip}(t) = b_{ip} \hat{y}_{ip}(t) + (1 - b_{ip}) \sum_{j \in N_i} b_{jp} \hat{y}_{jp}(t) \quad (16)$$

Step 3: Fusion function.

Following the previous steps, all available observational data is gathered by follower UAV  $i$ . However, this data is only locally available to UAV  $i$ ; thus, it is necessary to implement a module that consolidates all local observation data and outputs the synthesized result as the fused

observation data  $\tilde{y}_i$  for UAV  $i$ . This fused data is subsequently transmitted to the neighboring UAVs of  $i$  to contribute to the cooperative output.

Step 4: Check the performance of the fusion function.

Furthermore, the fused data must include the fault diagnosis result of the fused observation data  $\tilde{b}_{ip}$ , generated from  $b_{ip}$  and  $b_{jp}, j \in N_i$ . This inclusion is critical for the subsequent UAV's fusion function. It should be noted that the frequency of input fusion relies on the scale of the UAV network. Moreover, if the reliably fused observation data of the sensor still exhibit faults, implying that the sensor is an overlapping faulty sensor, the fused data must be reconstructed using the reconstruction model to further mitigate the fault. An overlapping faulty sensor indicates that all UAVs have experienced faults in the same sensor.

$$\tilde{b}_{ip} = b_{ip} \cdot \prod_{j \in N_i} b_{jp}. \quad (17)$$

**Remark 5.** This FTC framework introduces key innovations. It employs a decentralized BRB fault diagnosis model for accurate local fault identification under uncertainty. The core innovation is the distributed BRB-CF reconstruction model, which integrates fused neighbor data for enhanced input quality. For challenging overlapping faults where fusion is insufficient, it ensures accurate reconstruction via temporal integration. This combines current healthy fused data with historical information, using feedback from prior reconstructions, enabling estimation even without immediate observability. Advantages over existing methods (Yang and Dong, 2024; Han et al., 2018; Feng et al., 2023b) include distributed scalability, superior handling of overlapping faults compared to simple fusion, and robustness to model uncertainty via BRB's knowledge-data integration, unlike traditional model-based FTC. This synergy of decentralized diagnosis, intelligent communication-aware fusion, and adaptive BRB-CF reconstruction represents the main contribution to robust multi-UAV fault tolerance.

### 3.3. Optimization model of the BRB-based FTC framework

Above all, two BRB models are proposed, one is BRB model for fault diagnosis, another is BRB-CF model for reconstructing the faulty dimension of  $\tilde{y}_i$ . Their initialization is decided by experts. However, the initial parameters may not be the optimal parameters of models. In this way, the parameters decided by experts must be optimized in some way to fit the actual model not totally the experts' model. The optimization of BRB parameters including rule weights ( $\lambda_k, \zeta_k^p, \rho_k^p$ ), attribute weights ( $\delta_s, \tau_{l,p}, \nu_{r,p}$ ), and consequent belief degrees ( $\beta_{q,k}, \beta_{e,k}^p, \eta_{e,k}^p$ ) is a complex task crucial for model performance.

The Projection CMA-ES (P-CMA-ES) variant is specifically chosen here because it inherently incorporates mechanisms to handle the constraints that define the valid parameter space for BRB models. It projects candidate solutions back into the feasible region if they violate constraints during the search process. This direct handling of constraints within the algorithm ensures that all evaluated and final parameter sets are valid, which is more integrated and often more effective than using penalty methods commonly employed with other algorithms like standard GAs or PSO. Hence, P-CMA-ES is adapted to deal with this nonlinear, multi-objective optimization problem in this section.

For BRB-based fault diagnosis model, the optimization objective is to maximize the fault diagnosis accuracy. The fault diagnosis accuracy can be calculated as follows:

$$\zeta = \frac{S_t}{T_1}. \quad (18)$$

where  $T_1$  denotes the number of all the diagnosis times.  $S_t$  denotes the number of correct diagnosis times.

So the objective function to optimize this BRB model parameters can be profiled as:

$$\begin{aligned} & \max \zeta \\ & \text{s.t.} \\ & 0 \leq \beta_{q,k} \leq 1, \\ & 0 \leq \theta_k \leq 1, \\ & 0 \leq \delta_s \leq 1, \\ & \sum_{q=1}^Q \beta_{q,k} \leq 1. \end{aligned} \quad (19)$$

where  $\zeta$  represents the accuracy of the BRB-based fault diagnosis model.

For BRB-CF based reconstruction model, the optimization objective is to minimize the reconstruction error. The reconstruction error can be calculated as follows:

$$MSE^p = \frac{1}{K} \sum_{k=1}^K \left( y_{\text{actual}}^p(t_k) - \bar{y}_{\text{reconstructed}}^p(t_k) \right)^2. \quad (20)$$

where  $MSE^p$  represents the mean square error between the reconstructed  $p$ th dimension of fused observation data and the actual  $p$ th dimension of observation data from the  $p$ th sensor over  $K$  time samples  $t_k$ .

So the objective function to optimize the BRB-CF model parameters can be profiled as:

$$\begin{aligned} & \min MSE^p \\ & \text{s.t.} \\ & 0 \leq \beta_{e,k}^p, \eta_{e,k}^p \leq 1, \\ & 0 \leq \zeta_k^p, \rho_k^p \leq 1, \\ & 0 \leq \tau_{l,p}, \nu_{r,p} \leq 1, \\ & \sum_{e=1}^E \beta_{e,k}^p \leq 1, \quad \sum_{e=1}^E \eta_{e,k}^p \leq 1. \end{aligned} \quad (21)$$

## 4. Case study

This case study investigates the proposed distributed FTC framework using a system comprising one leader and four follower UAVs, so  $N = 4$ . This simulation scale is deemed sufficient to rigorously evaluate the framework's effectiveness under challenging conditions. A key advantage of this setup is the ability to explicitly simulate and analyze both sensor faults impacting single followers individually, and more complex scenarios where the same sensor fails simultaneously across multiple UAVs. Demonstrating robust performance in both these distinct cases serves to validate the core functionalities of the proposed approach: specifically, the distributed diagnosis using BRB, the fusion process based on communication, and the novel reconstruction mechanism using the BRB CF model, including its handling of observable Case 1 and unobservable Case 2 situations. Moreover, employing simulations with a limited number of agents to validate the fundamental performance of new distributed algorithms is a common and accepted practice within the multi-agent systems research community, as evidenced in related studies (Zhang et al., 2024b; Wang et al., 2022a). This focused approach allows for clear verification before exploring scalability in larger systems. The following subsections detail the system model, the specific fault scenarios implemented, the FTC framework configuration, and the simulation results.

**Table 2**

Reference points of four sensors in diagnosis model.

Reference point	L	M	H
Sensor 1 ( $p_x$ )	0	84	168
Sensor 2 ( $p_y$ )	0	35	70
Sensor 3 ( $v_x$ )	0	0.6	1.2
Sensor 4 ( $v_y$ )	0	0.25	0.5

#### 4.1. System description

The kinematic model of each follower UAV  $i$  (where  $i = 1, \dots, 4$ ) is defined by the following equations:

$$\begin{aligned} \dot{p}_{xi}(t) &= v_i(t) \cos \theta_i(t), \\ \dot{p}_{yi}(t) &= v_i(t) \sin \theta_i(t), \\ \dot{v}_i(t) &= -\frac{1}{T_i} v_i(t) + \frac{1}{T_i} g_i(t), \\ \dot{\theta}_i(t) &= \omega_i(t). \end{aligned} \quad (22)$$

where  $p_{xi}(t)$  and  $p_{yi}(t)$  represent the Cartesian coordinates of UAV  $i$ ,  $v_i(t)$  is the velocity,  $\omega_i(t)$  is the yaw angular velocity,  $g_i(t)$  is the velocity control input,  $\theta_i(t)$  is the yaw angle, and  $T_i$  is the velocity response time constant which is respectively set as:  $T_1 = 1.2, T_2 = 1.4, T_3 = 1.2, T_4 = 1.3$ .

Based on the dynamic feedback linearization the actual control input can be expressed by:

$$\begin{bmatrix} g_i(t) \\ \omega_i(t) \end{bmatrix} = \begin{bmatrix} T_i \cos \theta_i(t) & T_i \sin \theta_i(t) \\ -\frac{\sin \theta_i(t)}{v_i(t)} & \frac{\cos \theta_i(t)}{v_i(t)} \end{bmatrix} \begin{bmatrix} u_{xi}(t) \\ u_{yi}(t) \end{bmatrix}, \quad (23)$$

where  $u_i(t) = [u_{xi}(t) \ u_{yi}(t)]^T$  is the virtual input designed by:

$$u_i(t) = K_{1i}x_i(t) + K_{2i}\bar{y}_i(t) + K_{3i}(y_i(t) + h_i - \bar{y}_i(t)). \quad (24)$$

where  $x_i(t) = [p_{xi}(t) \ p_{yi}(t) \ v_{xi}(t) \ v_{yi}(t)]^T$  is the virtual state of UAV  $i$ ,  $K_{1i}$ ,  $K_{2i}$ , and  $K_{3i}$  are gain matrices to be designed.

It should be noted that the output of leader UAV is the state of leader UAV which means that the observer can be ignored in our case study.

The communication topology is shown in Fig. 3. For the formation control, the desired formation vectors are:

$$h_1 = [20 \ 0 \ 0 \ 0]^T, \quad h_2 = [40 \ 0 \ 0 \ 0]^T, \quad h_3 = [0 \ 10 \ 0 \ 0]^T, \quad h_4 = [0 \ 20 \ 0 \ 0]^T.$$

The controller gains are set as:

$$\begin{aligned} K_{11} = K_{13} &= \begin{bmatrix} -5 & 0 & -5.32 & 0 \\ 0 & -5 & 0 & -5.32 \end{bmatrix}, \\ K_{12} &= \begin{bmatrix} -5 & 0 & -5.62 & 0 \\ 0 & -5 & 0 & -5.62 \end{bmatrix}, \\ K_{14} &= \begin{bmatrix} -5 & 0 & -5.45 & 0 \\ 0 & -5 & 0 & -5.45 \end{bmatrix}, \quad K_{21} = K_{23} = \begin{bmatrix} 5 & 0 & 6.32 & 0 \\ 0 & 5 & 0 & 6.32 \end{bmatrix}, \\ K_{22} &= \begin{bmatrix} 5 & 0 & 6.64 & 0 \\ 0 & 5 & 0 & 6.64 \end{bmatrix}, \quad K_{24} = \begin{bmatrix} 5 & 0 & 6.45 & 0 \\ 0 & 5 & 0 & 6.45 \end{bmatrix}, \\ K_{31} = K_{32} = K_{33} = K_{34} &= \begin{bmatrix} -5 & 0 \\ 0 & -5 \end{bmatrix}. \end{aligned}$$

#### 4.2. Design of FTC framework for UAVs

This subsection details the specific configuration of the proposed FTC framework for the case study, focusing on handling both non-overlapping and overlapping sensor faults.

**Table 3**

Reference points of four sensors in case 2 reconstruction model.

Reference point	L	M	H
Sensor 1 ( $p_x$ )	19	75	140
Sensor 2 ( $p_y$ )	9	71	130
Sensor 3 ( $v_x$ )	0.999	1	1.004
Sensor 4 ( $v_y$ )	0.999	1	1.004

**Table 4**

Accuracy of fault-diagnosis model on each follower UAV.

UAV <sub>1</sub>	UAV <sub>2</sub>	UAV <sub>3</sub>	UAV <sub>4</sub>
100.00%	99.87%	99.88%	99.80%

The BRB models for fault diagnosis, introduced in Section 3.1, and reconstruction, described in Section 3.2, were constructed with reference points defined in Tables 2 and 3.

The simulation scenario involves a mission executed over a duration of 0–140 s. The following fault patterns are introduced:

$$M_1(t) = \begin{cases} \text{diag}(x, 1, 1, 1), & 20 \leq t < 40, \\ \text{diag}(1, x, 1, 1), & 40 \leq t \leq 60, \\ \text{diag}(1, 1, x, 1), & 60 < t < 80, \\ \text{diag}(1, 1, 1, x), & 80 < t < 100, \\ \text{diag}(x, 1, 1, 1), & 100 < t < 140. \end{cases} \quad (25)$$

$$M_2(t) = \begin{cases} \text{diag}(1, x, 1, 1), & 20 \leq t < 40, \\ \text{diag}(1, 1, x, 1), & 40 \leq t \leq 60, \\ \text{diag}(1, 1, x, 1), & 60 < t < 80, \\ \text{diag}(x, 1, 1, 1), & 80 < t < 100, \\ \text{diag}(x, 1, 1, 1), & 100 < t < 140. \end{cases} \quad (25)$$

$$M_3(t) = \begin{cases} \text{diag}(1, 1, x, 1), & 20 \leq t < 40, \\ \text{diag}(1, 1, 1, x), & 40 \leq t \leq 60, \\ \text{diag}(x, 1, 1, 1), & 60 < t < 80, \\ \text{diag}(1, x, 1, 1), & 80 < t < 100, \\ \text{diag}(x, 1, 1, 1), & 100 < t < 140. \end{cases} \quad (26)$$

$$M_4(t) = \begin{cases} \text{diag}(1, 1, 1, x), & 20 \leq t < 40, \\ \text{diag}(1, 1, 1, x), & 40 \leq t \leq 60, \\ \text{diag}(1, x, 1, 1), & 60 < t < 80, \\ \text{diag}(1, 1, x, 1), & 80 < t < 100, \\ \text{diag}(x, 1, 1, 1), & 100 < t < 140. \end{cases} \quad (26)$$

where  $x$  represents a faulty sensor whose output is scaled by a random multiplier drawn uniformly from [0, 1] at each time step within the specified fault interval. This simulates varying degrees of sensor degradation or failure. Note that the interval  $20 \leq t < 100$  s introduces various non-overlapping faults across the followers, while the interval  $100 \leq t < 140$  s presents a challenging overlapping fault scenario where sensor 1 fails simultaneously on all followers.

The training data for optimizing the BRB models was generated synthetically. For the FD module, datasets covering single faults in each of the four sensors, as well as no-fault conditions, were created over the 20–140 s time window using the random multiplier ‘ $x$ ’ for fault injection. For the reconstruction module, data covering the operational range during the 20–140 s interval was used.

The rule bases, including antecedent combinations, consequent belief degrees, rule weights, and attribute weights, were initialized based on expert knowledge and subsequently optimized using the P-CMA-ES algorithm against training data as described in Section 3.3. The final optimized parameters for the FD model and a reconstruction model for sensor 1 are provided in Tables 5 and 6.

**Table 5**

Optimized reconstruction model for the first sensor.

No.	Attribute			Rule weight	Output belief degree {L,M,H}	No.	Attribute			Rule weight	Output belief degree {L,M,H}
	A	B	D				A	B	D		
1	L	L	L	0.8409	{0.0223, 0.3931, 0.5846}	15	L	L	L	0.4554	{0.4167, 0.2618, 0.3215}
2	L	L	M	0.4974	{0.3988, 0.3175, 0.2837}	16	L	L	L	0.0095	{0.1668, 0.0315, 0.8017}
3	L	L	H	0.7986	{0.9034, 0.0657, 0.0309}	17	M	M	H	0.3785	{0.1139, 0.4594, 0.4267}
4	L	M	L	0.2874	{0.0572, 0.3293, 0.6134}	18	H	H	H	0.5777	{0.7650, 0.1270, 0.1080}
5	M	M	M	0.4211	{0.2051, 0.4452, 0.3497}	19	H	H	L	0.3684	{0.7821, 0.2043, 0.0136}
6	H	H	H	0.8258	{0.8180, 0.0950, 0.0870}	20	L	H	M	0.3048	{0.0247, 0.7131, 0.2622}
7	L	M	L	0.6146	{0.3605, 0.5842, 0.0553}	21	M	L	M	0.1623	{0.0796, 0.8155, 0.1048}
8	M	H	M	0.8814	{0.2890, 0.4509, 0.2601}	22	L	M	H	0.6103	{0.0000, 0.0057, 0.9949}
9	H	L	L	0.6413	{0.5045, 0.2834, 0.2122}	23	M	M	H	0.7919	{0.0807, 0.4774, 0.4419}
10	H	H	M	0.5266	{0.0667, 0.0283, 0.9050}	24	H	H	L	0.4740	{0.3601, 0.2975, 0.3423}
11	H	M	L	0.5874	{0.2823, 0.0927, 0.6251}	25	H	H	M	0.7911	{0.0005, 0.0031, 0.9964}
12	M	M	H	0.8585	{0.3355, 0.2878, 0.3768}	26	H	L	M	0.7008	{0.4031, 0.1561, 0.4408}
13	H	H	H	0.9207	{0.0419, 0.0415, 0.9166}	27	L	M	H	0.6886	{0.1039, 0.2709, 0.6252}
14	H	M	M	0.5244	{0.4309, 0.2781, 0.2910}						

**Table 6**

Optimized distributed FD model for one UAV.

No.	Attribute				Rule weight	Output belief degree {θ <sub>1</sub> , θ <sub>2</sub> , θ <sub>3</sub> , θ <sub>4</sub> , θ <sub>5</sub> }	No.	Attribute				Rule weight	Output belief degree {θ <sub>1</sub> , θ <sub>2</sub> , θ <sub>3</sub> , θ <sub>4</sub> , θ <sub>5</sub> }
	A	B	C	D				A	B	C	D		
1	L	L	L	L	0.4239	{0.0280, 0.0559, 0.1801, 0.1733, 0.5627}	42	M	M	M	H	0.9780	{0.1496, 0.0099, 0.6379, 0.1296, 0.0729}
2	L	L	L	M	0.1287	{0.1039, 0.1547, 0.3455, 0.0980, 0.2979}	43	M	M	H	L	0.3012	{0.0936, 0.0406, 0.2123, 0.2922, 0.3613}
3	L	L	L	H	0.3021	{0.1387, 0.2358, 0.3093, 0.1239, 0.1923}	44	M	M	H	M	0.8869	{0.0505, 0.1615, 0.0067, 0.5758, 0.2055}
4	L	L	M	L	0.5161	{0.1512, 0.0578, 0.1214, 0.2479, 0.4217}	45	M	M	H	H	0.0244	{0.1086, 0.2775, 0.1536, 0.0408, 0.4195}
5	L	L	M	M	0.5899	{0.1254, 0.0764, 0.2488, 0.4066, 0.1427}	46	M	H	L	L	0.3408	{0.0723, 0.0452, 0.5241, 0.0950, 0.2634}
6	L	L	M	H	0.3780	{0.1151, 0.0161, 0.5755, 0.1565, 0.1368}	47	M	H	L	M	0.9502	{0.2153, 0.3208, 0.1192, 0.2280, 0.1168}
7	L	L	H	L	0.1914	{0.1339, 0.0574, 0.2880, 0.2156, 0.3051}	48	M	H	L	H	0.2379	{0.0622, 0.0290, 0.1375, 0.7299, 0.0414}
8	L	L	H	M	0.9225	{0.0683, 0.2152, 0.0676, 0.3671, 0.2819}	49	M	H	M	L	0.6604	{0.1440, 0.0825, 0.6685, 0.0935, 0.0115}
9	L	L	H	H	0.1964	{0.1430, 0.1728, 0.1324, 0.3863, 0.1656}	50	M	H	M	M	0.1149	{0.2759, 0.1378, 0.1172, 0.3868, 0.0822}
10	L	M	L	L	0.7725	{0.4545, 0.1617, 0.0209, 0.1217, 0.0613}	51	M	H	M	H	0.5640	{0.0644, 0.3265, 0.3678, 0.1849, 0.0565}
11	L	M	L	M	0.7639	{0.0534, 0.0908, 0.0550, 0.5458, 0.2551}	52	M	H	H	L	0.4009	{0.0455, 0.6751, 0.1224, 0.0764, 0.0806}
12	L	M	L	H	0.1495	{0.0724, 0.3325, 0.0267, 0.2886, 0.2798}	53	M	H	H	M	0.1682	{0.2563, 0.1185, 0.4284, 0.1116, 0.0852}
13	L	M	M	L	0.6894	{0.0917, 0.2767, 0.2598, 0.3210, 0.0507}	54	M	H	H	H	0.5345	{0.5089, 0.0179, 0.1050, 0.0876, 0.2806}
14	L	M	M	M	0.6957	{0.4053, 0.2852, 0.1093, 0.0385, 0.1617}	55	H	L	L	L	0.2666	{0.0371, 0.5359, 0.0861, 0.1213, 0.2196}
15	L	M	M	H	0.5334	{0.1312, 0.3677, 0.3257, 0.0048, 0.1707}	56	H	L	L	M	0.1688	{0.1885, 0.2090, 0.3990, 0.0971, 0.1065}
16	L	M	H	L	0.3235	{0.0706, 0.0588, 0.4569, 0.2102, 0.2034}	57	H	L	H	H	0.7791	{0.3900, 0.2948, 0.1024, 0.1030, 0.1099}
17	L	M	H	M	0.7594	{0.0639, 0.1589, 0.2788, 0.1990, 0.2994}	58	H	L	M	L	0.2502	{0.1895, 0.0436, 0.1425, 0.3646, 0.2597}
18	L	M	H	H	0.7727	{0.4382, 0.0487, 0.1295, 0.1548, 0.2288}	59	H	L	M	M	0.9375	{0.1159, 0.2032, 0.1917, 0.4072, 0.0819}
19	L	H	L	L	0.8666	{0.2155, 0.1184, 0.2095, 0.2099, 0.2466}	60	H	L	M	H	0.2814	{0.1426, 0.1037, 0.1500, 0.4856, 0.1181}
20	L	H	L	M	0.5604	{0.4188, 0.0518, 0.1328, 0.2620, 0.1345}	61	H	L	H	L	0.8429	{0.1222, 0.1197, 0.2206, 0.0831, 0.4544}
21	L	H	L	H	0.6667	{0.2872, 0.2342, 0.1930, 0.1481, 0.1376}	62	H	L	H	M	0.8486	{0.3058, 0.0426, 0.1763, 0.2413, 0.2340}
22	L	H	M	L	0.5615	{0.0121, 0.6252, 0.0575, 0.0399, 0.2653}	63	H	L	H	H	0.6053	{0.0616, 0.2806, 0.3724, 0.1199, 0.1655}
23	L	H	M	M	0.4462	{0.0650, 0.0753, 0.4335, 0.1696, 0.2566}	64	H	M	L	L	0.5397	{0.0757, 0.2653, 0.1108, 0.1400, 0.4083}
24	L	H	M	H	0.8740	{0.1657, 0.0262, 0.2449, 0.1124, 0.4509}	65	H	M	L	M	0.5174	{0.1342, 0.4279, 0.0169, 0.0957, 0.3253}
25	L	H	H	L	0.9081	{0.0677, 0.1512, 0.4710, 0.2119, 0.0982}	66	H	M	L	H	0.1543	{0.0212, 0.3005, 0.1865, 0.0751, 0.4167}
26	L	H	H	M	0.4495	{0.2880, 0.1454, 0.1679, 0.2754, 0.1234}	67	H	M	M	L	0.4518	{0.0870, 0.5063, 0.0959, 0.1056, 0.2051}
27	L	H	H	H	0.6114	{0.3218, 0.2823, 0.0541, 0.1505, 0.1913}	68	H	M	M	M	0.3701	{0.0958, 0.3549, 0.1310, 0.2181, 0.2001}
28	M	L	L	L	0.3649	{0.3330, 0.2974, 0.2236, 0.0550, 0.0910}	69	H	M	H	M	0.8214	{0.0872, 0.1515, 0.2105, 0.3576, 0.1933}
29	M	L	L	M	0.8383	{0.1626, 0.0729, 0.2535, 0.1816, 0.3294}	70	H	M	H	L	0.4164	{0.0956, 0.0898, 0.1002, 0.5336, 0.1807}
30	M	L	L	H	0.8129	{0.2324, 0.6152, 0.0109, 0.0826, 0.0588}	71	H	M	H	M	0.1017	{0.1826, 0.0675, 0.5624, 0.1805, 0.0070}
31	M	L	M	L	0.9171	{0.1054, 0.0515, 0.2632, 0.2957, 0.2841}	72	H	M	H	H	0.6045	{0.0485, 0.4385, 0.0246, 0.2677, 0.2207}
32	M	L	M	M	0.7624	{0.0869, 0.1683, 0.0874, 0.4923, 0.1650}	73	H	H	L	L	0.7547	{0.4019, 0.2023, 0.0628, 0.2321, 0.1009}
33	M	L	M	H	0.2423	{0.0398, 0.2363, 0.2767, 0.0727, 0.3746}	74	H	H	L	M	0.3384	{0.2220, 0.0509, 0.0908, 0.2836, 0.3527}
34	M	L	H	L	0.3672	{0.5176, 0.1369, 0.2531, 0.0300, 0.0624}	75	H	H	L	H	0.1771	{0.0837, 0.0340, 0.5655, 0.0246, 0.2922}
35	M	L	H	M	0.8968	{0.4548, 0.1155, 0.1138, 0.2247, 0.0912}	76	H	H	M	L	0.6299	{0.2140, 0.1749, 0.1493, 0.3184, 0.1434}
36	M	L	H	H	0.6448	{0.0322, 0.5311, 0.0517, 0.1143, 0.2707}	77	H	H	M	M	0.7615	{0.1713, 0.1476, 0.1257, 0.2562, 0.2992}
37	M	M	L	L	0.0499	{0.1304, 0.1519, 0.4253, 0.2371, 0.0553}	78	H	H	M	H	0.3646	{0.2180, 0.0630, 0.4149, 0.1372, 0.1669}
38	M	M	L	M	0.2814	{0.0902, 0.2035, 0.0162, 0.2077, 0.4823}	79	H	H	L	M	0.3196	{0.0769, 0.4454, 0.0395, 0.2975, 0.1407}
39	M	M	L	H	0.9514	{0.1889, 0.1225, 0.1958, 0.0318, 0.4609}	80	H	H	H	M	0.7955	{0.1647, 0.1593, 0.0846, 0.3525, 0.2389}
40	M	M	M	L	0.5063	{0.1382, 0.2140, 0.2316, 0.1277, 0.2886}	81	H	H	H	H	0.1108	{0.1566, 0.2433, 0.2488, 0.1084, 0.2431}

The simulation results of FD module have been shown in Fig. 4 and Table 4. Fig. 4 illustrates the performance of the distributed FD module, detailed in Section 3.1. The figure presents results for each follower UAV, labeled UAV 1 to UAV 4, operating under the specific fault conditions defined in Eqs. (25) and (26). The horizontal axis represents time, while the vertical axis shows the diagnosed “Failure Condition”. The labels on this axis signify the system state identified by the FD module. Specifically, F-1, F-2, F-3, and F-4 correspond to detected faults primarily associated with sensors 1, 2, 3, and 4 respectively. The label

F-5 represents the diagnosed “No Fault” or “All Healthy” state. The blue lines within each subplot track the fault state diagnosed by the module as it evolves over time. Red dots indicate instances of misdiagnosis, where the module’s output did not align with the actual injected fault state. For example, the module sometimes diagnosed F-5 “No Fault” when sensor 1 was actually faulty, particularly between 100 and 140 s for UAVs 2, 3, and 4. The apparent density of red dots in certain intervals can be attributed to the high sampling frequency used throughout the simulation period, even though the overall diagnostic accuracy

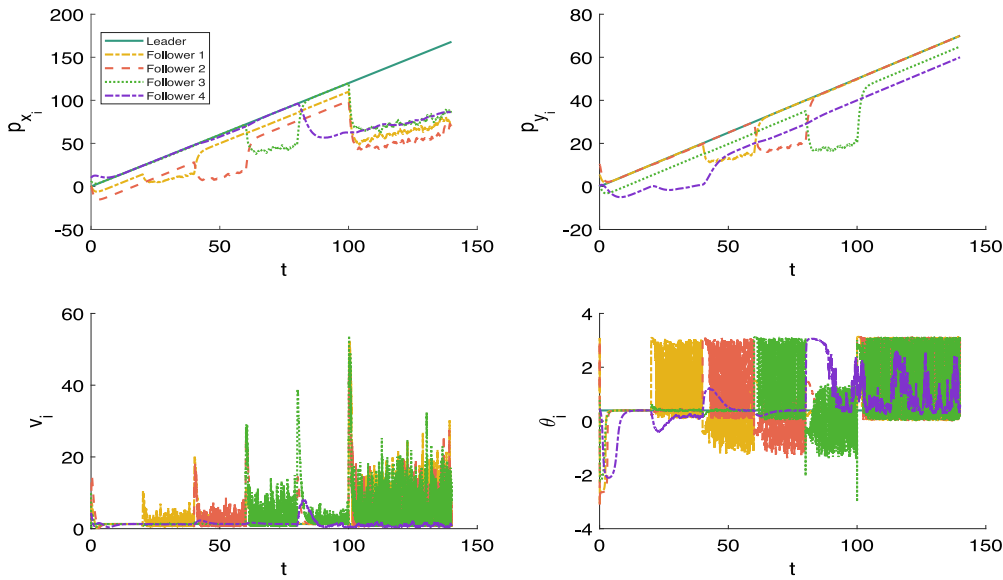


Fig. 9. UAVs' states under failure.

remains high. Overall, the results presented in Fig. 4 demonstrates the diagnosis module's capability to successfully track the dynamically changing fault conditions for the vast majority of time steps. Moreover, it can be observed from Table 4 that high diagnostic accuracies were achieved for the respective UAVs: 100%, 99.87%, 99.88%, and 99.80%. These ensure timely and generally accurate fault identification, which is crucial for subsequent fault-tolerant actions within the system.

Fig. 5 shows the fault injection following the pattern mentioned above. As depicted, the output of each affected sensor randomly oscillates between 0 and its original value during fault periods. Fig. 6 illustrates the reconstructed outputs generated by the distributed FTC framework for each sensor on each follower UAV under these various fault conditions.

During the 20–100 s interval, each follower UAV suffers from a different, non-overlapping sensor fault. For these cases, the reconstructed output is produced by the fusion function, which relies on the communication network. The sensor faults are effectively tolerated through communication between UAVs, leveraging the inherent sensor redundancy across the team, where healthy sensors on neighboring UAVs provide substitute data.

From 100–140 s, all follower UAVs experience the same overlapping fault in sensor 1, corresponding to the leader UAV's x-position. Based on the definition of joint observability, during this time period, the system condition for joint observability using only fused neighbor data is not satisfied. Thus, historical data from sensor 1 is utilized by the BRB-CF reconstruction model described as Case 2 in Section 3.2.1 to provide necessary information for estimation.

As seen in Fig. 6, there are some deviations in the reconstructed signals. These deviations are primarily caused by instances of incorrect diagnosis from the FD module, which are visible as errors in Fig. 4. At these specific time points, the FTC mechanisms, specifically fusion or reconstruction, do not engage correctly, allowing the faulty data to persist momentarily. Since diagnostic accuracy can rarely be a perfect 100

Fig. 7 clearly demonstrates the detrimental effect of uncompensated sensor faults, showing erratic trajectories and a complete loss of the desired formation. In contrast, Fig. 8 depicts the system's behavior when the proposed distributed FTC framework is active. Despite the occurrence of both non-overlapping and overlapping faults, particularly sensor 1 during 100–140 s, affecting all followers, the UAVs successfully maintain the overall formation structure.

The fusion mechanism effectively handles non-overlapping faults using neighbor data during 20–100 s, while the BRB-CF reconstruction

mitigates the overlapping faults, albeit with some minor oscillations visible during the 100–140 s interval, likely due to the inherent difficulty of reconstruction from limited data and occasional diagnosis imperfections (as seen in Fig. 4). And these oscillations are mainly caused by some incorrect diagnosis even though the diagnosis accuracy is over 99.8%.

Comparing the state trajectories, Fig. 9 reveals significant divergence and oscillations in positions ( $p_{xi}$ ,  $p_{yi}$ ) and velocities ( $v_{xi}$ ,  $v_{yi}$ ) for all follower UAVs under fault conditions without the FTC scheme, indicating instability. Notably, during the 100–140 s interval, the  $p_x$  state of all follower UAVs diverges significantly from the leader's trajectory. This is specifically caused by the overlapping fault in sensor 1, meaning no healthy measurement or estimate of the leader's  $p_x$  state is available to any follower without fault compensation.

Conversely, Fig. 10 demonstrates the effectiveness of the proposed FTC framework in reconstructing the faulty sensor readings. During the 20–100 s period, the non-overlapping sensor faults are handled perfectly by the fusion function using neighbor data, resulting in smooth state trajectories with no need for the BRB-based reconstruction model. Even during the challenging 100–140 s interval with the overlapping sensor 1 fault, the states remain bounded and track the leader's state (offset by the formation vectors). However, some oscillations are noticeable, particularly in the velocity states ( $v_{xi}$ ,  $v_{yi}$ ), during this latter period (100–140 s). These are primarily attributed to instances of misdiagnosis by the distributed BRB diagnosis model. Such momentary diagnostic errors cause brief periods where the controller receives uncompensated or incorrectly compensated data, leading to transient control adjustments as the followers momentarily struggle but ultimately succeed in maintaining the correct formation. Overall, Fig. 10 clearly shows the framework's ability to preserve system stability and formation accuracy under both non-overlapping and overlapping fault conditions, despite minor imperfections in diagnosis.

## 5. Conclusion

This paper proposes a distributed FTC framework for multi-UAV systems with faulty sensors, leveraging a BRB approach for fault diagnosis and reconstruction. The developed FTC framework successfully addresses both overlapping and non-overlapping sensor faults by using distributed BRB models for real-time fault management. Simulation results demonstrate the framework's ability to maintain UAV formation and performance despite sensor failures. The proposed distributed FTC

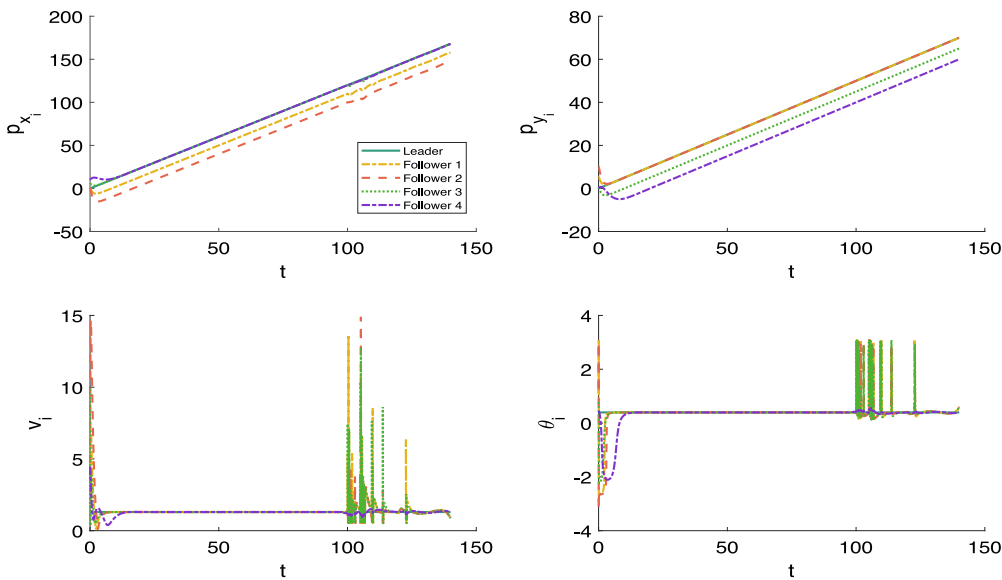


Fig. 10. UAVs' states using proposed FTC.

framework enhances the robustness and fault tolerance of multi-UAV systems, providing a scalable and resilient solution for various practical applications such as disaster management, environmental monitoring, and surveillance. This research contributes to the field of autonomous systems, offering new insights and methodologies for robust fault management capabilities. Possible future works will extend our BRB-based FTC framework to multi-UAVs subject to interferences and a broader range of fault types, such as bias, drift, unboundedness.

#### CRediT authorship contribution statement

**Ruohan Yang:** Writing – Review & editing, Supervision, Methodology, Conceptualization. **Xiao Gong:** Writing – Original Draft, Software, Formal analysis, Data curation, Conceptualization. **Zhichao Feng:** Visualization, Validation, Supervision, Methodology, Resources. **Yahui Hao:** Visualization, Validation, Project administration.

#### Funding

This study was funded partly by National Natural Science Foundation of China under Grant No. 62203365 and No. 62203461, partly by Aeronautical Science Foundation under Grant 2023Z034053004, partly by China Postdoctoral Science Foundation under Grant No. 2023M742843, partly by the Young Talent Promotion Program of Shaanxi Association for Science and Technology under Grant No. 20220121, 20230125.

#### Declaration of competing interest

The authors declare that they have no known competing financial interests or personal relationships that could have appeared to influence the work reported in this paper.

#### Data availability

The authors are unable or have chosen not to specify which data has been used.

#### References

- Ahmadi, K., Asadi, D., Merheb, A., Nabavi-Chashmi, S.-Y., Tutsoy, O., 2023. Active fault-tolerant control of quadrotor uavs with nonlinear observer-based sliding mode control validated through hardware in the loop experiments. *Control Eng. Pract.* 137, 105557.
- AlMahamid, F., Grolinger, K., 2022. Autonomous unmanned aerial vehicle navigation using reinforcement learning: A systematic review. *Eng. Appl. Artif. Intell.* 115, 105321.
- Baldini, A., Felicetti, R., Ferracuti, F., Freddi, A., Iarlori, S., Monterù, A., 2023. Real-time propeller fault detection for multirotor drones based on vibration data analysis. *Eng. Appl. Artif. Intell.* 123, 106343.
- Chang, L., Xu, X., Liu, Z.-g., Qian, B., Xu, X., Chen, Y.-W., 2020. BRB prediction with customized attributes weights and tradeoff analysis for concurrent fault diagnosis. *IEEE Syst. J.* 15 (1), 1179–1190.
- Du, Z., Zhang, H., Wang, Z., Yan, H., 2024. Fuzzy model predictive formation maneuver control of multi-UAVs with interval output-constrained. *IEEE Trans. Fuzzy Syst.*
- Feng, Z., He, W., Zhou, Z., Ban, X., Hu, C., Han, X., 2020. A new safety assessment method based on belief rule base with attribute reliability. *IEEE/ CAA J. Autom. Sin.* 8 (11), 1774–1785.
- Feng, Z., Yang, R., Zhou, Z., Hu, C., 2023a. Trustworthy fault diagnosis method based on belief rule base with multisource uncertain information for vehicle. *IEEE Trans. Ind. Electron.* 71 (7), 7947–7956.
- Feng, Z., Zhou, Z.-J., Hu, C., Chang, L., Hu, G., Zhao, F., 2018. A new belief rule base model with attribute reliability. *IEEE Trans. Fuzzy Syst.* 27 (5), 903–916.
- Feng, Z., Zhou, Z., Yang, R., Ban, X., Hu, C., 2023b. Fault-tolerant control based on belief rule base expert system for multiple sensors concurrent failure in liquid launch vehicle. *Nonlinear Dynam.* 111 (5), 4357–4373.
- Gong, J., Jiang, B., Ma, Y., Mao, Z., 2022. Distributed adaptive fault-tolerant formation control for heterogeneous multiagent systems with communication link faults. *IEEE Trans. Aerosp. Electron. Syst.* 59 (2), 784–795.
- Guo, X.-G., Ahn, C.K., 2020. Adaptive fault-tolerant pseudo-pid sliding-mode control for high-speed train with integral quadratic constraints and actuator saturation. *IEEE Trans. Intell. Transp. Syst.* 22 (12), 7421–7431.
- Han, J., Liu, X., Wei, X., Zhu, X., 2023a. Reduced-order observer-based finite time fault estimation for switched systems with lager and fast time varying fault. *IEEE Trans. Circuits Syst. II: Express Briefs* 71 (1), 350–354.
- Han, J., Liu, X., Xie, X., Wei, X., 2023b. Dynamic output feedback fault tolerant control for switched fuzzy systems with fast time varying and unbounded faults. *IEEE Trans. Fuzzy Syst.* 31 (9), 3185–3196.
- Han, W., Trentelman, H.L., Wang, Z., Shen, Y., 2018. A simple approach to distributed observer design for linear systems. *IEEE Trans. Autom. Control* 64 (1), 329–336.
- Li, Y., Xu, T., Yang, R., Wang, M., 2023. Distributed adaptive finite-time fault-tolerant formation-containment control for networked euler-lagrange systems under directed communication interactions. *Neurocomputing* 560, 126839.
- Ma, Y., Jiang, B., Wang, J., Gong, J., 2023. Adaptive fault-tolerant formation control for heterogeneous uavs-ugvs systems with multiple actuator faults. *IEEE Trans. Aerosp. Electron. Syst.* 59 (5), 6705–6716.
- Queraltà, J.P., Taipalmaa, J., Pullinen, B.C., et al., 2020. Collaborative multi-robot search and rescue: Planning, coordination, perception, and active vision. *IEEE Access* 8, 191617–191643.

- Rotondo, D., Theilliol, D., Ponsart, J.C., 2023. Virtual actuator and sensor fault tolerant consensus for homogeneous linear multi-agent systems. *IEEE Trans. Circuits Syst. I. Regul. Pap.* 71 (3), 1324–1334.
- Shao, X., Ye, D., 2020. Fuzzy adaptive event-triggered secure control for stochastic nonlinear high-order mass subject to dos attacks and actuator faults. *IEEE Trans. Fuzzy Syst.* 29 (12), 3812–3821.
- Sun, Q., Liu, W., Cai, L., 2025. Multi-dynamic target coverage tracking control strategy based on multi-UAV collaboration. *Control Eng. Pract.* 155, 106170.
- Wang, Z., Li, S., He, W., Yang, R., Feng, Z., Sun, G., 2022a. A new topology-switching strategy for fault diagnosis of multi-agent systems based on belief rule base. *Entropy* 24 (11), 1591.
- Wang, C., Wen, X., Niu, Y., et al., 2018. Dynamic task allocation for heterogeneous manned-unmanned aerial vehicle teamwork. In: 2018 Chinese Automation Congress. CAC, IEEE, pp. 3345–3349.
- Wang, Y., Yan, M., Feng, G., Qin, S., Wei, F., 2023. Autonomous on-demand deployment for UAV assisted wireless networks. *IEEE Trans. Wirel. Commun.* 22 (12), 9488–9501.
- Wang, X., Zhou, Y., Huang, T., Chakrabarti, P., 2022b. Event-triggered adaptive fault-tolerant control for a class of nonlinear multiagent systems with sensor and actuator faults. *IEEE Trans. Circuits Syst. I. Regul. Pap.* 69 (10), 4203–4214.
- Xu, X., Feng, G., Qin, S., Liu, Y., Sun, Y., 2023. Joint UAV deployment and resource allocation: a personalized federated deep reinforcement learning approach. *IEEE Trans. Veh. Technol.*
- Xu, X., Yan, X., Sheng, C., Yuan, C., Xu, D., Yang, J., 2017. A belief rule-based expert system for fault diagnosis of marine diesel engines. *IEEE Trans. Syst. Man Cybern. - A: Syst. Hum.* 50 (2), 656–672.
- Yadegar, M., Meskin, N., 2021. Fault-tolerant control of nonlinear heterogeneous multi-agent systems. *Automatica* 127, 109514.
- Yang, W., Dong, J., 2024. Distributed fault-tolerant consensus for one-sided lipschitz multiagent systems based on error decomposition and jointly observable condition. *Inform. Sci.* 657, 119994.
- Yang, J.-B., Liu, J., Wang, J., Sii, H.-S., Wang, H.-W., 2006. Belief rule-base inference methodology using the evidential reasoning approach-rimer. *IEEE Trans. Syst. Man Cybern.- A: Syst. Hum.* 36 (2), 266–285.
- Yang, R., Su, X., Li, Y., Zhang, S., Zhou, D., 2023a. Distributed event-triggered simultaneous fault detection and consensus control for multiple lur'e systems. *IEEE Syst. J.*
- Yang, R., Su, X., Zhang, S., Zhou, D., Feng, Z., 2023b. Simultaneous fault detection and leader-following consensus for multi-agent systems with directed graphs via dynamic event-triggered strategy. *IEEE Trans. Instrum. Meas.*
- Yang, W., Xu, S., Chen, X., Chai, Y., 2024. Diagnosis of current sensors incipient faults in three phase three-level npc rectifiers based on adaptive sliding mode observer. *IEEE Sens. J.*
- Zhang, B., Lin, X., Zhu, Y., Tian, J., Zhu, Z., 2024a. Enhancing multi-UAV reconnaissance and search through double critic ddpg with belief probability maps. *IEEE Trans. Intell. Veh.*
- Zhang, H., Yang, R., He, W., Feng, Z., 2024b. Cooperative performance assessment for multiagent systems based on the belief rule base with continuous inputs. *Inform. Sci.* 676, 120815.
- Zhang, C., Zhou, Z., Ning, P., Zhang, P., Lian, Z., Ming, Z., 2024c. IBRNet: Interpretable Belief Rule Network modeling method for fault diagnosis of redundant inertial navigation systems. *Control Eng. Pract.* 144, 105822.
- Zhang, C., Zhou, Z., Ning, P., Zhang, P., Lian, Z., Ming, Z., 2024d. MBRB: Micro-belief rule base model based on cautious conjunctive rule for interpretable fault diagnosis. *Eng. Appl. Artif. Intell.* 137, 105557.
- Zheng, B.-C., Guo, L., Li, K., 2021. Event-triggered sliding mode fault-tolerant consensus for a class of leader-follower multi-agent systems. *Int. J. Control. Autom. Syst.* 19 (8), 2664–2673.
- Zou, W., Ahn, C.K., Xiang, Z., 2020. Fuzzy-approximation-based distributed fault-tolerant consensus for heterogeneous switched nonlinear multiagent systems. *IEEE Trans. Fuzzy Syst.* 29 (10), 2916–2925.